

Non-perturbative renormalization of asymmetric staple-shaped operators in twisted mass lattice QCD

Constantia Alexandrou,^{1,2,*} Simone Bacchio,² Krzysztof Cichy,³ Martha Constantinou,⁴ Xu Feng,^{5,6,7} Karl Jansen,⁸ Chuan Liu,^{5,6,7} Aniket Sen,^{9,10,†} Gregoris Spanoudes,^{1,2} Fernanda Steffens,^{9,10} and Jacopo Tarello^{1,2}

¹*Department of Physics, University of Cyprus, P.O. Box 20537, 1678 Nicosia, Cyprus*

²*Computation-based Science and Technology Research Center,
The Cyprus Institute, 20 Kavafi Str., Nicosia 2121, Cyprus*

³*Faculty of Physics, Adam Mickiewicz University,
ul. Uniwersytetu Poznańskiego 2, 61-614 Poznań, Poland*

⁴*Temple University, 1925 N. 12th Street, Philadelphia, PA 19122-1801, USA*

⁵*School of Physics and State Key Laboratory of Nuclear Physics and Technology, Peking University, Beijing 100871, China*

⁶*Collaborative Innovation Center of Quantum Matter, Beijing 100871, China*

⁷*Center for High Energy Physics, Peking University, Beijing 100871, China*

⁸*NIC, DESY, Platanenallee 6, D-15738 Zeuthen, Germany*

⁹*Helmholtz Institut für Strahlen- und Kernphysik,
Rheinische Friedrich-Wilhelms-Universität Bonn, Nussallee 14-16, 53115 Bonn*

¹⁰*Bethe Center for Theoretical Physics, Rheinische Friedrich-Wilhelms-Universität Bonn, Nussallee 12, 53115 Bonn, Germany*

(Dated: May 22, 2023)

Staple-shaped Wilson line operators are necessary for the study of transverse momentum-dependent parton distribution functions (TMDPDFs) in lattice QCD and beyond. In this work, we study the renormalization of such operators in the general case of an asymmetric staple. We analyze the mixing pattern of these operators using their symmetry properties, where we find that the possible mixing is restricted within groups of four operators. We then present numerical results using the regularization independent scheme, RI/MOM, to study the importance of mixing using one operator in particular, the γ_0 operator. Based on these results, we consider the short distance ratio (SDR) scheme, which is desirable in the absence of mixing. Finally, we investigate a variant of the RI/MOM scheme, where the renormalization factors are computed at short distances.

PACS numbers:

I. INTRODUCTION

Collinear parton distribution functions (PDFs) probe the hadron structure from the perspective of the spin and longitudinal momentum distributions of the quarks and gluons that make up the hadron. The vast amount of work to determine these distributions over the last five decades, both theoretically and experimentally, has enormously expanded our view of the hadron structure, the proton in particular [1]. And yet, these developments are mostly limited to probing the one-dimensional structure of the proton. In order to have a wider understanding of the proton structure, we also need to understand how the momentum and the spin are distributed in the transverse plane. For that, we need to measure and compute the generalized parton distributions and the transverse-momentum-dependent PDFs (TMDPDFs), the latter being the main focus of this present work. Although there has been an effort to obtain TMDPDFs from phenomenological fits to experimental data [2–7], their accuracy is still far from being at the same level as the collinear PDFs. This status will change in the coming years with new data coming from Jefferson Lab [8] and from the future Electron-Ion-Collider to be built at Brookhaven National Lab [9]. It is, thus, of great importance to extract TMDPDFs from first principles calculations, namely, lattice QCD.

In the last 10 years, there has been an enormous advance in computing the collinear PDFs using lattice QCD [10–18]. By comparison, the computation of TMDPDFs is still in its infancy [19–22], although progress has been made in the computation of key elements required to build the TMDPDFS, like the soft functions [23, 24] and the Collins-Soper

*Electronic address: alexand@ucy.ac.cy

†Electronic address: sen@hiskp.uni-bonn.de

kernel [25–27]. Such computations have been restricted to ratios of TMDPDFs [28–31], and only recently, a first full lattice QCD calculation of the TMDPDFs themselves has been presented [32]. One fundamental difficulty in these calculations is to have control over the renormalization procedure, which is more involved than in the case of collinear PDFs. In particular, the staple-shaped gauge link that enters in the evaluation of TMDPDFs has three types of divergences: i) linear divergence coming from the Wilson line, which connects the quark fields and which depends on the length of the staple-shaped link; ii) logarithmic divergences coming from the endpoints of the staple link, similarly to the case of straight gauge links; and iii) logarithmic divergences coming from the presence of cusps in the staple. In addition, in the limit of infinite-length staple, L , (which is the case of interest), pinch-pole singularities arise as positive powers of L , coming from the gluon exchange between the transverse segments of the staple. Moreover, as in the case of straight gauge links, staple-shaped operators of different Dirac structures can and will mix on the lattice among certain groups (when chiral symmetry is broken), as dictated by discrete symmetries. However, in this case, the mixing pattern of the operators employed in lattice regularization can be significantly more involved than in the case of the straight Wilson line.

A first study within lattice perturbation theory to one-loop for the case of the symmetric staple [33] showed mixing between certain pairs of Dirac structures. The mixing depended solely on the direction of the staple link entering the end points of the staple regardless of the shape of the staple. This implies that the same mixing pattern occurs also for asymmetric staple shapes. In Ref. [34], the mixing pattern of these staple-shaped operators¹ has been studied using symmetry considerations. It was found that more mixing is present than observed in Ref. [33]. This demonstrates that one-loop perturbation theory cannot fully reveal the mixing of the staple operators, unlike the case of straight Wilson-line operators [35], and a higher-loop computation is needed to confirm the additional mixing patterns found by symmetry arguments. The authors of Refs. [23, 27, 36] examined 16 independent projectors in the RI-type prescription for each Dirac structure. While Ref. [27] identified several finite contributions in the asymmetric staple-shaped operator, Ref. [23, 36] found negligible contributions, at least at small transverse separations, by setting specific momentum components to be zero. However, we emphasize that this does not imply nonzero mixing, as these finite contributions may appear in the Green's functions defined in the continuum and, thus, vanish in the renormalization prescription that requires the difference between lattice and continuum expressions. Additional finite contributions can also arise due to mixing with higher dimensional operators of different Dirac structures which vanish in the continuum limit. Moreover, these contributions are of higher twist and are disregarded in the present calculation. In this work, we use symmetry arguments to restrict the set of operators that are allowed to mix.

The common conclusion of these studies is that there are remaining non-perturbative divergences in the RI/MOM scheme that make it hard to renormalize at large transverse separations. An alternative approach that one can adopt is the so-called *ratio scheme* as proposed for the quasi-PDF case [11, 37, 38]. In this approach, one subtracts the Ultra-Violet (UV) divergences by taking the ratio with a suitable object at a fixed short distance, where perturbation theory applies. Many choices of suitable objects for the ratio have been proposed in Ref. [39]. The authors of Refs. [32, 36] choose the same matrix element but at zero longitudinal momentum for taking the ratio and name this scheme as *short distance ratio* (SDR). As for the remaining divergences associated with the asymmetric staple-shaped link, one can cancel them by taking an appropriate ratio with the vacuum expectation value of a rectangular Wilson loop [40]. However, we would like to stress that the SDR scheme is valid when operator mixing is absent or negligible. We check that in the case under study the mixing is indeed negligible and thus, one can employ the ratio scheme. Another option, as proposed in Ref. [34], is to employ RI/MOM in the spirit of the SDR scheme by fixing the dimensions of the staple at a short perturbative range (we will call this scheme RI-short).

The paper is organized as follows. Section II discusses how TMDs can be accessed on a Euclidean lattice using the quasi-distribution approach. In Section III, we study operator mixing using symmetry arguments. Section IV presents our lattice setup. The size of the mixing is examined in Section V. In Sections V A, V B and V C we employ RI/MOM, SDR and RI-short schemes, respectively, by following the procedures described in Ref. [32, 34, 36]. In Section VI, we present the renormalized beam functions in the three renormalization schemes discussed here, and then show the corresponding results in the $\overline{\text{MS}}$ scheme. The conclusions are presented in Section VII.

II. QUASI-TMDPDFS

A first-principle computation of TMDPDFs in the context of LaMET is more involved than collinear PDFs. The main obstacle is to correctly subtract the so-called rapidity divergences, which are associated with the soft gluon radiation

¹ For conciseness, we will refer to staple-shaped Wilson quark bilinear operators as staple-shaped operators.

of the infinitely long Wilson lines present in the staple-shaped operator. This subtraction is made through the use of a soft function [41, 42]. Different ways how to perform this subtraction in the context of LaMET can be found in Ref. [43]. In general, the TMD soft function involves two opposite light-like directions, and this makes a lattice calculation significantly challenging. In Refs. [21, 40], the authors define a rapidity-independent reduced soft function S_r and show that it can be extracted from a form factor and the quasi-TMD wave function of a light meson. Using S_r , the rapidity scheme-independent TMDPDF $f^{TMD}(x, b, \mu, \zeta)$ can be written as [15, 40]

$$f^{TMD}(x, b, \mu, \zeta) = H\left(\frac{\zeta_z}{\mu^2}\right) e^{-\ln\left(\frac{\zeta_z}{\mu^2}\right)K(b, \mu)} \tilde{f}(x, b, \mu, \zeta_z) S_r^{\frac{1}{2}}(b, \mu) + \dots \quad (1)$$

where $\tilde{f}(x, b, \mu, \zeta_z)$ is the so-called quasi-TMDPDF, x is the longitudinal momentum fraction, b the transverse separation. The scale μ defines the renormalization scale and $\zeta_z = (2xP^z)^2$ is the Collins-Soper scale of the quasi-TMDPDF, with ζ being the scale for the light-cone correlation. The factor $H\left(\frac{\zeta_z}{\mu^2}\right)$ is the perturbative matching kernel that perturbatively connects the TMDPDFs to the quasi-TMDPDFs, and $K(b, \mu)$ is the Collins-Soper kernel. The renormalization scheme in Eq. (1) is left unspecified; usually, it is computed in the $\overline{\text{MS}}$ scheme. The quasi-TMDPDF on the lattice is defined as [20, 43]

$$\tilde{f}(x, b, \mu, \zeta_z) = \lim_{L \rightarrow \infty} \int \frac{dz}{2\pi} e^{-iz\zeta_z} \frac{P^z}{E_P} B(z, b, L, P^z, \mu). \quad (2)$$

Here, $B(z, b, P^z)$ is known as the quasi-beam function, and it is defined in terms of a bare matrix element with a non-local quark bilinear operator as

$$B_{0,\Gamma}(z, b, L, P^z) = \langle N(P^z) | \mathcal{O}^\Gamma(z, b, L) | N(P^z) \rangle \quad (3)$$

$$= \langle N(P^z) | \bar{\psi}(b+z) \Gamma \mathcal{W}(b+z; L) \psi(0) | N(P^z) \rangle, \quad (4)$$

where $N(P^z)$ is a nucleon state with momentum boost of $(0, 0, P^z)$ and $\psi(x)$ is the standard up and down quark doublet. For the unpolarized TMDPDF, Γ can be either γ_0 or γ_3 or in general a combination of the two. In this work, we show results for $\Gamma = \gamma_0$, since we observe a better signal for this operator compared to $\Gamma = \gamma_3$. γ_0 was also used for the quasi-PDF case, strongly due to this operator being free from any mixing, while γ_3 mixed with $\mathbf{1}$. In the case of the staple, however, no such advantage exists, as will be shown in Section III. In general, the asymmetric staple-shaped Wilson, $\mathcal{W}(b+z; L)$, is given by:

$$\begin{aligned} \mathcal{W}(b+z; L) &= W_z(\vec{x}; L) W_\perp(\vec{x} + L\hat{z}; b) W_z(\vec{x} + L\hat{z} + b\hat{y}; -L+z), \\ W_z(\vec{x}; L) &= \mathcal{P} \exp \left[-ig \int_0^L d\lambda \hat{z} \cdot A(\vec{x} + \hat{z}\lambda) \right]. \end{aligned} \quad (5)$$

with L the length of the symmetric part, and x an arbitrary point, while W_z defines a Wilson line along the boost direction and W_\perp defines one along the transverse direction. The shape of the asymmetric staple is shown in Fig. 1.

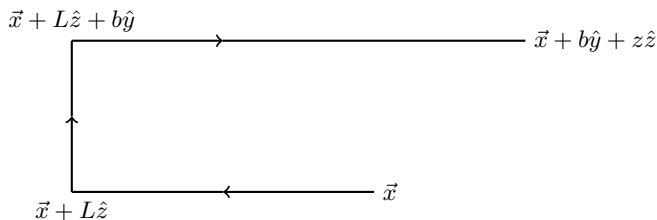


FIG. 1: The shape of the asymmetric staple defined in the operator of the quasi-beam function

III. OPERATOR MIXING THROUGH SYMMETRY

In order to use symmetry arguments to determine which operators mix, we first organize the staple-shaped operator using all possible ways to connect the fermion fields. We show in Fig. 2 two of the possible ways to connect the quark

and antiquark fields with coordinates (\hat{y}, \hat{z}) . In this notation, b is always in the \hat{y} direction, while L and z are in the \hat{z} direction. We define the operator shown on the left of Fig. 2 as $O^{++}(\Gamma)$, where the two plus signs define the positive direction of the Wilson line along transverse (\hat{y}) and longitudinal (\hat{z}) axes. Under this notation, the operator shown on the right of Fig. 2 is $O^{+-}(\Gamma)$. We have two other possibilities, $O^{-+}(\Gamma)$ and $O^{--}(\Gamma)$, along with the corresponding charge-conjugated operators, leading to a total of eight operators. The charge conjugated operators O_C are given by the same geometry as that of the original staple, only with the path going in the opposite direction. Thus, $O_C^{++}(\Gamma)$ is also given by the left staple of Fig. 2, only the arrows are in the opposite direction, and similarly for the remaining three operators. In the case of the symmetric staple ($z = 0$), the charge-conjugated operators are redundant.

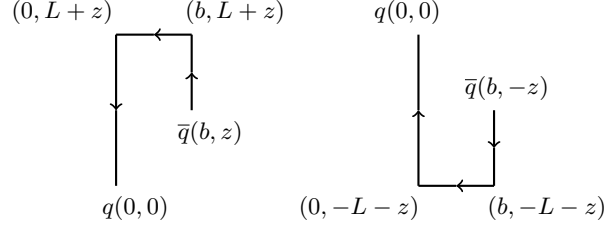


FIG. 2: The shape of the asymmetric staple defined in the operator of the quasi-beam function

We analyze the symmetry properties using generalized parity and time reversal with discrete flavor rotation, and charge conjugation for the fermion fields in the twisted mass basis, $\chi(x_\alpha, \mathbf{x})$, and the gauge link, $U(x_\alpha, \mathbf{x}; \alpha)$, in some direction α . The generalized parity in the α -direction combined with discrete flavor rotation [44] is then given by

$$\mathcal{P}_{F\alpha}^{1,2} : \begin{cases} U(x_\alpha, \mathbf{x}; \alpha) \rightarrow U(x_\alpha, -\mathbf{x}; \alpha), \\ U(x_\alpha, \mathbf{x}; \beta \neq \alpha) \rightarrow U^{-1}(x_\alpha, -\mathbf{x} - a\hat{\beta}; \beta), \\ \chi(x_\alpha, \mathbf{x}) \rightarrow i\gamma_\alpha \tau_{1,2} \chi_l(x_\alpha, -\mathbf{x}), \\ \bar{\chi}(x_\alpha, \mathbf{x}) \rightarrow -i\bar{\chi}(x_\alpha, -\mathbf{x}) \tau_{1,2} \gamma_\alpha, \end{cases} \quad (6)$$

where the "standard" parity is the one with $\alpha = 0$, and the 3-vector \mathbf{x} is what remains from the 4-vector x after removing x_α . $\tau_{1,2}$ are the Pauli spin matrices in flavor space. Similarly, the generalized time reversal combined with discrete flavor rotation is given by

$$\mathcal{T}_{F\alpha}^{1,2} : \begin{cases} U(x_\alpha, \mathbf{x}; \alpha) \rightarrow U^{-1}(-x_\alpha - a, \mathbf{x}; \alpha), \\ U(x_\alpha, \mathbf{x}; \beta \neq \alpha) \rightarrow U(-x_\alpha, \mathbf{x}; \beta), \\ \chi(x_\alpha, \mathbf{x}) \rightarrow i\gamma_\alpha \gamma_5 \tau_{1,2} \chi_l(-x_\alpha, \mathbf{x}), \\ \bar{\chi}(x_\alpha, \mathbf{x}) \rightarrow -i\bar{\chi}(-x_\alpha, \mathbf{x}) \tau_{1,2} \gamma_5 \gamma_\alpha. \end{cases} \quad (7)$$

Finally, the charge conjugation transformation is given by

$$\mathcal{C} : \begin{cases} U(x) \rightarrow (U^\dagger(x))^T, \\ \chi(x) \rightarrow C^{-1} \bar{\chi}(x)^T, \\ \bar{\chi}(x) \rightarrow -\chi(x)^T C. \end{cases} \quad (8)$$

To study the symmetry properties, we need to consider all eight different staple-shaped operators. To summarize the effect of the transformations, we use the notation $(ijkl)_c$. Here i, j, k, l denote the signs of $O^{++}, O^{--}, O^{+-}, O^{-+}$ and $c = \pm$ denotes the sign of the charge conjugated operators ($c = +$ if it stays the same, $c = -$ if it is opposite). The relevant combinations that have definite symmetry properties are:

$$\begin{aligned} (+ + + +)_c &\equiv (- - - -)_c, \\ (+ - + -)_c &\equiv (- + - +)_c, \\ (+ + - -)_c &\equiv (- - + +)_c, \\ (+ - - +)_c &\equiv (- + + -)_c. \end{aligned}$$

As an example, we look at the symmetry properties of γ_0 and $\gamma_0\gamma_3$ given in Tables I and II, respectively. The Dirac structure Γ' is the transformation applied to the insertion Dirac structure Γ , and we restrict ourselves here to the flavor non-singlet case, τ_3 . The combination of operators that mix are:

$$\begin{aligned} & (+ + + +)_c \text{ with } (+ - - +)_c, \\ & (+ - + -)_c \text{ with } (+ + - -)_c, \\ & (+ + - -)_c \text{ with } (+ - + -)_c, \\ & (+ - - +)_c \text{ with } (+ + + +)_c. \end{aligned}$$

Although we show the resulting mixing pattern only for the γ_0 and $\gamma_0\gamma_3$ cases, this mixing holds true for all pairs $(\Gamma, \Gamma\gamma_3)$. The symmetry properties for all Γ 's are summarized in Table IV in Appendix A. Based on this, we conclude that the possible mixing is between Γ and $\{\Gamma\gamma_2, \Gamma\gamma_3, \Gamma\gamma_2\gamma_3\}$. Since, in this work, we only consider $\Gamma = \gamma_0$, the relevant mixing for us is between γ_0 and $\{\gamma_0\gamma_2, \gamma_0\gamma_3, \gamma_5\gamma_1\}$.

We point out that different mixing patterns have been considered in recent studies of other groups, including mixing among all 16 operators of different Dirac structures [27], or at least mixing in pairs $(\Gamma, \Gamma\gamma_3)$ [34]. In our work, we choose to consider the minimal set of staple-shaped operators (of the same dimension) that are allowed to mix by the above-mentioned C, P, and T symmetries. We have not considered mixing with higher-dimensional operators allowed by Lorentz symmetry (see, e.g., Ref. [45] for the straight Wilson-line case), since it is power suppressed and not relevant when one takes the continuum limit $a \rightarrow 0$. This can explain the nonzero (but small) mixings among certain Dirac structures observed in Ref. [27]. Also, in contrast to Ref. [34], in our analysis, the staple line has been chosen to be in a 2-dimensional (D), and not 3D, plane in Euclidean space formed by the transverse (\hat{y}) and longitudinal (\hat{z}) directions. In this respect, we end up with a basis of 8 (instead of 16) operators, which are eigenstates of C, P and T transformations. We also note that calculations in one-loop lattice perturbation theory [33] show a smaller mixing pattern compared to the symmetries; however, this cannot guarantee a reduced mixing in higher loops.

	Γ'	$(+ + + +)_c$ $(- - - -)_c$	$(+ - + -)_c$ $(- + - +)_c$	$(+ + - -)_c$ $(- - + +)_c$	$(+ - - +)_c$ $(- + + -)_c$
$\mathcal{P}_{F0}^{1,2}$	γ_0	-	+	-	+
$\mathcal{P}_{F1}^{1,2}$	$-\gamma_0$	+	-	+	-
$\mathcal{P}_{F2}^{1,2}$	$-\gamma_0$	+	+	-	-
$\mathcal{P}_{F3}^{1,2}$	$-\gamma_0$	+	-	-	+
$\mathcal{T}_{F0}^{1,2}$	$-\gamma_0$	+	+	+	+
$\mathcal{T}_{F1}^{1,2}$	γ_0	-	-	-	-
$\mathcal{T}_{F2}^{1,2}$	γ_0	-	+	+	-
$\mathcal{T}_{F3}^{1,2}$	γ_0	-	-	+	+
C	γ_0	c	c	c	c

TABLE I: Symmetry properties of γ_0 .

IV. LATTICE SETUP

For the lattice simulation, we use an $N_f = 2 + 1 + 1$ clover-improved twisted mass fermion ensemble of size $24^3 \times 48$, produced by the Extended Twisted Mass Collaboration (ETMC) [46]. Our study is done using N_{conf} configurations with N_{src} source positions for each configuration. To increase statistics, the boost is taken in all three directions, and both positive and negative. For each such direction of boost, the staple is then constructed in both the remaining transverse directions. This gives us 12 measurements (6 boost directions \times 2 transverse directions) for each source position. The details of the lattice simulation are summarized in Table III.

	Γ'	$(++++)_c$ $(----)_c$	$(+ - + -)_c$ $(- + - +)_c$	$(+ + - -)_c$ $(- - + +)_c$	$(+ - - +)_c$ $(- + + -)_c$
$\mathcal{P}_{F0}^{1,2}$	$-\gamma_0\gamma_3$	+	-	+	-
$\mathcal{P}_{F1}^{1,2}$	$\gamma_0\gamma_3$	-	+	-	+
$\mathcal{P}_{F2}^{1,2}$	$\gamma_0\gamma_3$	-	-	+	+
$\mathcal{P}_{F3}^{1,2}$	$-\gamma_0\gamma_3$	+	-	-	+
$\mathcal{T}_{F0}^{1,2}$	$-\gamma_0\gamma_3$	+	+	+	+
$\mathcal{T}_{F1}^{1,2}$	$\gamma_0\gamma_3$	-	-	-	-
$\mathcal{T}_{F2}^{1,2}$	$\gamma_0\gamma_3$	-	+	+	-
$\mathcal{T}_{F3}^{1,2}$	$-\gamma_0\gamma_3$	+	+	-	-
C	$-\gamma_0\gamma_3$	c	c	c	c

TABLE II: Symmetry properties of $\gamma_0\gamma_3$.

Lattice size	a [fm]	$a\mu_l$	m_π [MeV]	N_{conf}	N_{src}	N_{meas}
$24^3 \times 48$	0.093	0.00530	350	100	8	9600

TABLE III: We give the parameters of the lattice ensemble and measurements used in the calculation. a is the lattice spacing, μ_l is the bare twisted light quark mass, m_π the pion mass, N_{conf} the number of configurations, N_{src} the number of source positions and N_{meas} the total number of measurements.

The bare matrix element for the quasi-beam function is calculated through a ratio of a 3-point to a 2-point function,

$$\begin{aligned}
B^\Gamma(z, b, L, P^z) &= \frac{\langle C_\Gamma^{3pt}(z, b, L, P^z; t_s, \tau) \rangle}{\langle C^{2pt}(P^z; t_s) \rangle} \\
&= \frac{\mathcal{P} \sum_{\mathbf{x}} e^{-i\mathbf{P}\cdot\mathbf{x}} \langle 0 | N(\mathbf{x}, t_s) \mathcal{O}^\Gamma(z, b, L; \tau) \bar{N}(\mathbf{0}, 0) | 0 \rangle}{\mathcal{P} \sum_{\mathbf{x}} e^{-i\mathbf{P}\cdot\mathbf{x}} \langle 0 | N(\mathbf{x}, t_s) \bar{N}(\mathbf{0}, 0) | 0 \rangle},
\end{aligned} \tag{9}$$

where τ is the insertion time of the operator \mathcal{O}^Γ and t_s defines the source-sink time separation. \mathcal{P} is the parity projector. In this work, we show results for a single source-sink separation of $t_s = 10a$ and a longitudinal momentum of $P^z = 6\pi/24a \sim 1.7$ GeV.

The 3-point function is constructed for the isovector combination $u - d$, by inserting a τ_3 in flavor space. This choice ensures the elimination of the disconnected contributions and only connected diagrams need to be calculated.

Momentum smearing [47] is applied to improve the signal for large boosts. It is observed that applying stout smearing to the gauge links used in construction of the staple also reduces the statistical errors. Here, we have applied 5 steps of stout smearing to the staple-shaped Wilson line.

In Fig. 3 we show the bare matrix elements as a function of z at a fixed $b/a = 1$ for different values of L . We notice that the real part of the matrix elements are symmetric in the simultaneous change $z \rightarrow -z$, $b \rightarrow -b$, while the imaginary part is anti-symmetric, for fixed P^z . For $P^z > 0$, we use the operator O^{++} for $z > 0$, and the operator O_c^{--} for $z < 0$. Using these properties, we symmetrize our results between positive and negative values of z . Our results show a clear divergence in L , as expected [15]. In Fig. 4 we show the dependence of the bare beam function on b . As expected [15], it decays exponentially with b .

V. NON-PERTURBATIVE RENORMALIZATION

As in the case of the straight Wilson line, there are logarithmic and linear divergences associated with the length z of the staple-shaped link. However, here there are two extra divergences: one, which is associated with the cusps of the staple, and one associated with the gluon exchange between the gauge links of length $L \rightarrow \infty$, the so-called pinch-pole singularities. On the other hand, the finite transverse separation b mitigates possible discretization effects associated with small z separation, mainly in the nonperturbative region (large b), which is the main interest of a lattice calculation. In the following, we will analyze three different ways to carry out the renormalization, namely

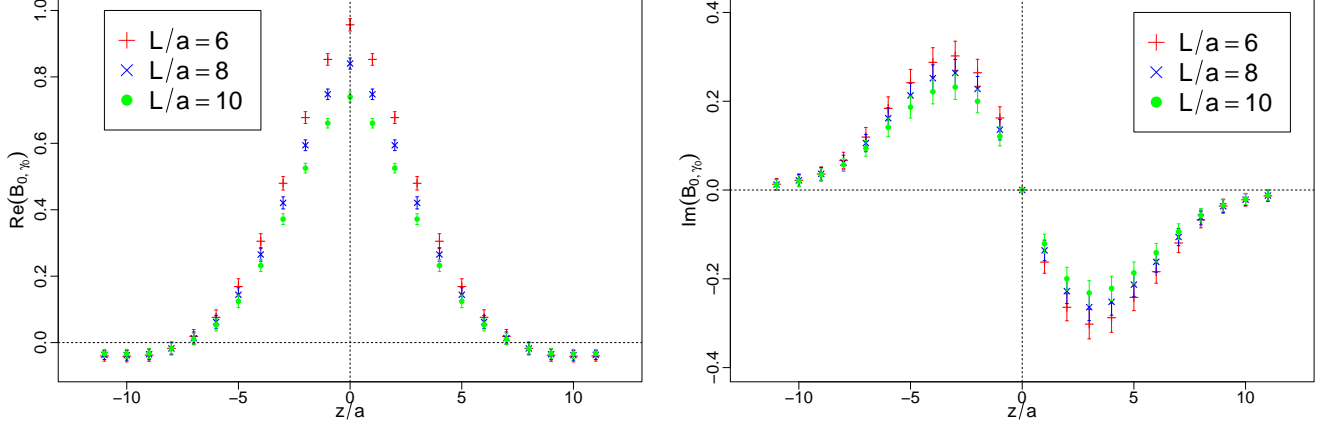


FIG. 3: Real and imaginary parts of the bare matrix elements for a transverse separation of $b/a = 1$.

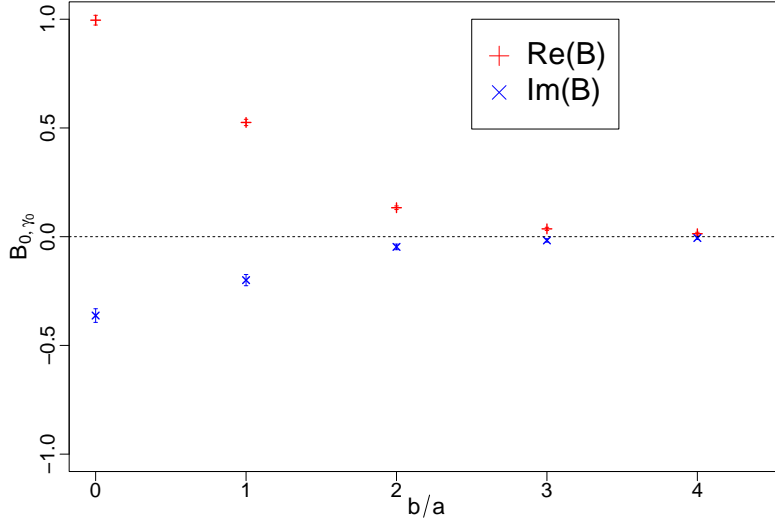


FIG. 4: Dependence of the bare matrix element on the transverse separation b for $L/a = 10$ and $z/a = 2$.

the RI/MOM scheme, the short distance ratio scheme, and a modified version of the RI/MOM scheme, where the renormalization constants are computed at short distances.

A. RI/MOM

The RI/MOM scheme [48] was first adapted for non-local operators employed in the quasi-distribution approach in Refs. [35, 49]. The RI/MOM renormalization constants $Z_{\mathcal{O}}^{\text{RI}}$ are defined by the condition

$$\frac{Z_{\mathcal{O}}^{\text{RI}}(z, b, L, \mu_0; 1/a)}{Z_q^{\text{RI}}(\mu_0; 1/a)} \frac{1}{12} \text{Tr} \left[\frac{\Lambda_0^\Gamma(z, b, L, p; 1/a) \Gamma'}{e^{ip^z z + ip_\perp b}} \right] \Bigg|_{p^2 = \mu_0^2} = 1, \quad (10)$$

where Λ_0^Γ is defined in terms of the amputated Green's function

$$\Lambda_0^\Gamma(z, b, L, p; 1/a) = S_q^{-1} G^\Gamma(z, b, L, p; 1/a) S_q^{-1}, \quad (11)$$

with S_q the off-shell quark propagator. The Green's function is calculated as

$$G^\Gamma(z, b, p, L; 1/a) = \langle q(p) | \mathcal{O}^\Gamma(z, b, p, L; 1/a) | q(p) \rangle. \quad (12)$$

Because G^Γ , and thus Λ^Γ , have the same divergences as $B_{0,\Gamma}$, all the divergences, in principle, cancel in the renormalization procedure. Z_q^{RI} is the quark wave function renormalization defined as

$$Z_q^{\text{RI}}(\mu_0; 1/a) = \frac{1}{12} \text{Tr} [(S_q(p; 1/a))^{-1} S_q^{\text{Born}}(p)] \Big|_{p^2=\mu_0^2}, \quad (13)$$

and the corresponding renormalized beam function is then

$$B_\Gamma^{\text{RI}}(z, b, \mu_0, P^z) = \sum_{\Gamma'} [Z_{\mathcal{O}}^{\text{RI}}(z, b, \mu_0; 1/a)]_{\Gamma\Gamma'} B_{0,\Gamma'}(z, b, P^z; 1/a). \quad (14)$$

The case of interest in this work is $\Gamma = \gamma_0$, computed using the lattice ensemble of Table III. As pointed out in Section III, γ^0 mixes with $\gamma_0\gamma_2$, $\gamma_0\gamma_3$, and $\gamma_5\gamma_1$. The renormalization factors for the diagonal and off-diagonal cases are shown in Figs. 5 and 6, respectively. As can be seen, the contributions from the off-diagonal mixing terms are $\lesssim 4\%$ of the diagonal contribution for all z when $b = 1a, 2a$.

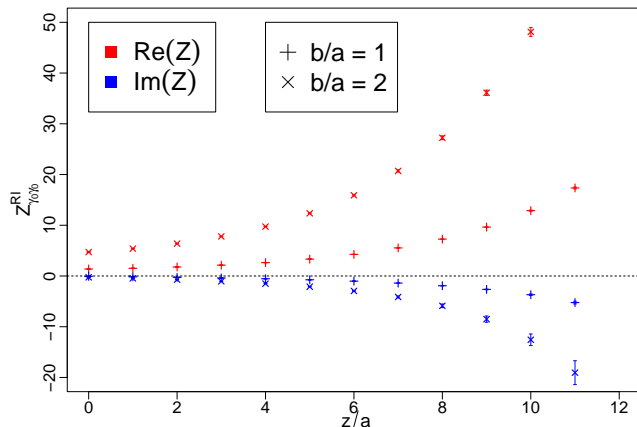


FIG. 5: Divergence of the RI/MOM renormalization factor as a function of z for $b/a = 1, 2$ and at fixed $L/a = 10$.

It is interesting to examine how the relative size of the off-diagonal to the diagonal renormalization factors changes as b increases, as the primary focus of lattice computation of TMDPDFs is the non-perturbative region in the transverse separation b . We show in Fig. 7 the renormalization factors as a function of b for the diagonal and off-diagonal contributions. We see a contribution of $\lesssim 7-8\%$ up to $b = 6a$ for the off-diagonal terms. Although their size shows a possible tendency of growth with increasing b , this growth seems to be only moderate. We notice that the authors of Ref. [27] considered the entire set of Dirac structures for the operator mixing, and observe similar results to ours, where only the relevant operators allowed by symmetry were used. The contribution from $\gamma_5\gamma_1$ is much larger than that of $\gamma_0\gamma_2$ and $\gamma_0\gamma_3$, and there is a steady increase going to larger b values. The magnitude of mixing for these operators found in Ref. [27] is also comparable to our findings. However, considering the dominant diagonal renormalization factors, it seems that there are remaining divergences related to large values of z and b , as also observed in Ref. [36]. Combined with the fact that the bare matrix element decays exponentially with b [15], it is significantly hard to renormalize for large transverse separations using this scheme. However, in the small b region where we can extract information using RI/MOM, it can be confirmed that the mixing is negligible. As an example, we show in Fig. 8 the renormalized beam function for the $b = 1a$ case, with circles denoting the RI/MOM procedure using the full mixing matrix and with the triangles denoting the case of only taking into account the diagonal contribution. Considering that including the mixing has a negligible effect, one can safely ignore operator mixing for these values of b .

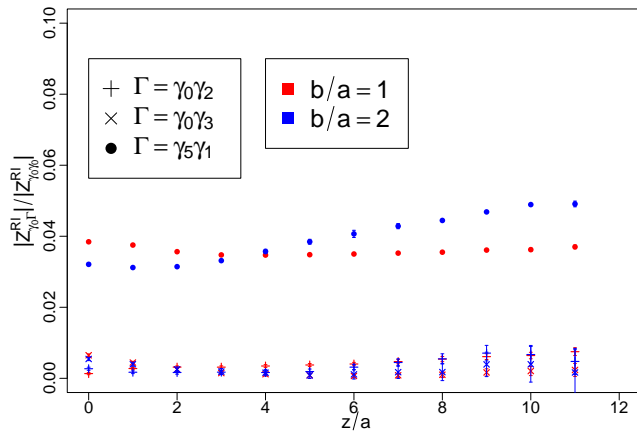


FIG. 6: Contribution of the off-diagonal mixing terms compared to the diagonal one, in the RI/MOM renormalization matrix at fixed $L/a = 10$.

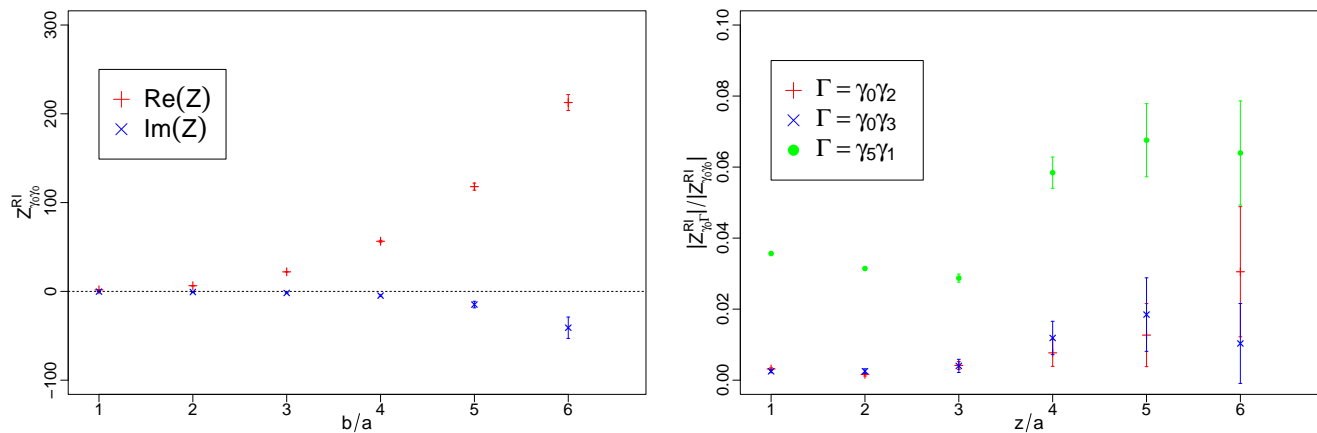


FIG. 7: The diagonal and off-diagonal contributions to the RI/MOM renormalization factors as a function of b at fixed $L/a = 10$ and $z/a = 2$.

B. The short distance ratio scheme

According to Figs. 6 and 7, mixing with different operators can be neglected at least up to $b/a \lesssim 6$, and we can assume that the renormalization of the staple-shaped link is multiplicative. This justifies the approach taken in Refs. [32, 36]. We first note that the vacuum expectation value of a rectangular Wilson loop Z_E with sides $2L + z$ and b ,

$$Z_E(b, 2L + z; 1/a) = \frac{1}{3} \text{Tr} \langle 0 | \mathcal{W}(b; 2L + z) W_{\perp}(x + b; b) | 0 \rangle, \quad (15)$$

has, by construction, the same divergences as that of the staple-shaped gauge link as defined in Eq. (5). Thus, it should cancel the pinch-pole singularity associated with the length L of the staple, as well as the divergences associated with the cusps. Furthermore, as the sides of Z_E are also dependent on the longitudinal displacement z , the exponential divergence associated with z present in the staple-shaped link must also be cancelled if an appropriated ratio is taken, namely the one proposed in Refs. [21, 36]:

$$B_{\Gamma}(z, b, P^z; 1/a) = \lim_{L \rightarrow \infty} \frac{B_{0,\Gamma}(z, b, L, P^z; 1/a)}{\sqrt{Z_E(b, 2L + z; 1/a)}} \quad (16)$$

To illustrate this point, we show in Fig. 9 the beam function as a function of L , for a fixed $z = 2a$ and two values of b , before and after dividing by $\sqrt{Z_E}$. The cancellation of the divergences related to the length of the Wilson line

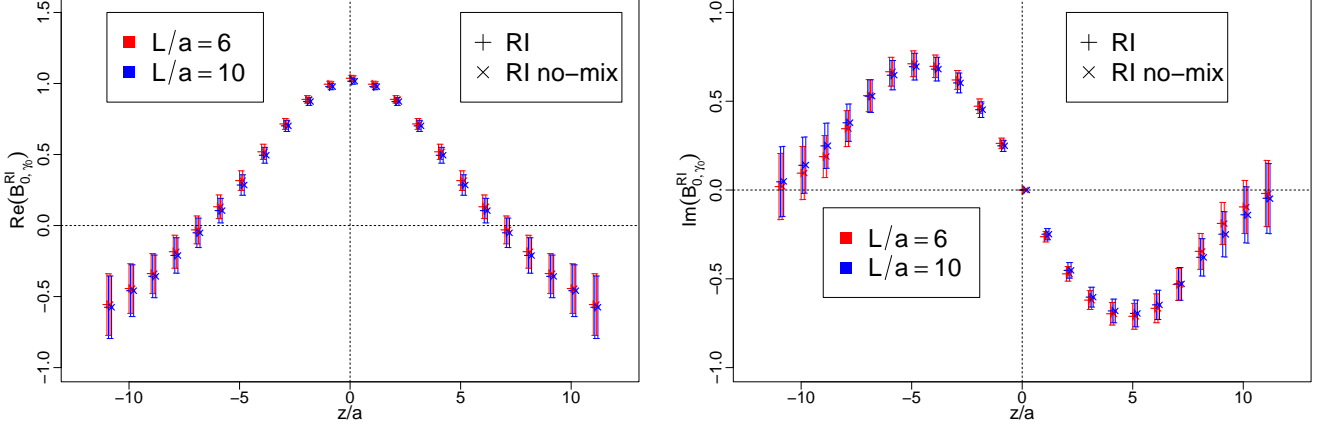


FIG. 8: Real and imaginary parts of the RI/MOM renormalized matrix elements for a transverse separation of $b/a = 1$.

is explicitly shown. This ratio, thus, takes care of the divergence associated with the length L and width b of the staple-shaped operator.

After dividing the beam function by the square root of Z_E , the only remaining divergences are the UV divergences

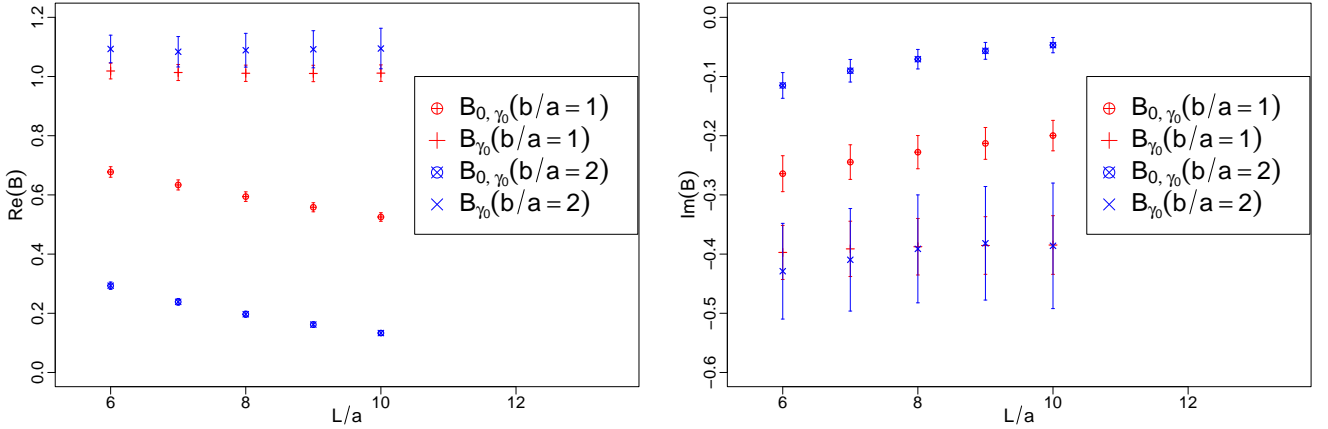


FIG. 9: The effect of taking the ratio of the bare matrix elements with $\sqrt{Z_E}$ at a fixed $z/a = 2$.

associated with the quark field and its end-points connecting to the gauge links. As such, they can be cancelled by taking ratios, as they have a multiplicative nature [26, 50]. Hence, one can define

$$B_{\Gamma}^{SDR}(z, z_0, b, b_0, P^z) = Z^{SDR}(z_0, b_0; 1/a) B_{\Gamma}(z, b, P^z; 1/a), \quad (17)$$

where,

$$Z^{SDR}(z_0, b_0; 1/a) = \frac{1}{B_{\Gamma}(z = z_0, b = b_0, P^z = 0; 1/a)}. \quad (18)$$

Because the remaining divergences are independent of the length of the Wilson line, one is free to choose z_0 and b_0 . However, because we want to connect these quantities to the $\overline{\text{MS}}$ scheme via a perturbative scheme conversion, z_0 and b_0 should be small enough for perturbation theory to be valid.

The renormalized matrix elements are converted to the $\overline{\text{MS}}$ scheme using perturbation theory. We have computed the vertex, sail, and tadpole one-loop diagrams for external quark states with a general momentum p^z . For $p^z \rightarrow 0$,

we obtain

$$Z^{\overline{\text{MS}},\text{SDR}}(z_0, b_0, \mu_0) = 1 + \frac{\alpha_s C_F}{2\pi} \left(\frac{1}{2} + \frac{3}{2} \ln \left(\frac{b_0^2 + z_0^2}{4e^{-2\gamma_E} \mu_0^2} \right) - 2 \frac{z_0}{b_0} \arctan \frac{z_0}{b_0} \right), \quad (19)$$

which agrees with Eq. (6) of Ref. [36]. Note that this factor equals $B_{\Gamma}^{\overline{\text{MS}}}(z = z_0, b = b_0, P^z = 0, \mu_0)$. Details of this calculation for a general external momentum will be presented in Ref. [51]. The renormalized beam function in the $\overline{\text{MS}}$ scheme is then given by

$$B_{\Gamma}^{\overline{\text{MS}}}(z, b, P^z) = Z^{\overline{\text{MS}}}(z_0, b_0, \mu_0) B_{\Gamma}^{\text{SDR}}(z, z_0, b, b_0, P^z). \quad (20)$$

Results for $B^{\overline{\text{MS}}}(z, b, P^z)$ are presented in Section VI, where we also discuss the cancellation of the z_0, b_0 dependence in Eq. (20).

C. Short distance RI/MOM

As discussed in Section V A, the usual RI scheme may be problematic at large z and b as the magnitude of the Z^{RI} factors grows exponentially. Also, as shown in Refs. [36, 52], the usual RI scheme may still contain a residual linear divergence, which may not be properly canceled. On the other hand, as discussed in Section V B, the $\sqrt{Z_E}$ factor cancels all divergences in z and b present in the staple. Hence, we can define a vertex function that is free of such divergences,

$$\Lambda^{\Gamma}(z, b, p; 1/a) = \frac{\Lambda_0^{\Gamma}(z, b, p; 1/a)}{\sqrt{Z_E(b, 2L + z; 1/a)}}. \quad (21)$$

Because the divergences related to the lengths of the Wilson line have been removed, we can compute the renormalization factors as in Section V B at some fixed z_0, b_0 [34]

$$\frac{Z_{\mathcal{O}}^{\text{RI-short}}(z_0, b_0, \mu_0; 1/a)}{Z_q^{\text{RI}}(\mu_0; 1/a)} \frac{1}{12} \text{Tr} \left[\frac{\Lambda^{\Gamma}(z, b, p; 1/a) \Gamma'}{e^{ip^z z + ib p_{\perp}}} \right] \Big|_{p^2 = \mu_0^2, z = z_0, b = b_0} = 1. \quad (22)$$

(23)

In principle, one can do this subtraction from the vertex in the standard RI/MOM. This would reduce the growth of the Z -factors with increasing b . However, in combining Z^{RI} with the bare B_{γ_0} , the $\sqrt{Z_E}$ factor cancels, and therefore this subtraction has no effect on the renormalized matrix elements. But if we fix the RI/MOM factors at a short perturbative scale, then this subtraction must be performed in order to cancel the cusp and linear divergences.

As in Section V B, we choose the pair z_0, b_0 to be in the perturbative region in order to make the perturbative conversion to the $\overline{\text{MS}}$ scheme reliable. We label this procedure RI-short. The corresponding renormalized beam function in this scheme is then given by

$$B_{\Gamma}^{\text{RI-short}}(z, z_0, b, b_0, \mu_0, P^z) = \sum_{\Gamma'} [Z_{\mathcal{O}}^{\text{RI-short}}(z_0, b_0, \mu_0; 1/a)]_{\Gamma\Gamma'} B_{\Gamma'}(z, b, P^z; 1/a). \quad (24)$$

For illustration, we show in Fig 10 the renormalization factors $Z_{\mathcal{O}}^{\text{RI-short}}(z_0, b_0, \mu_0; 1/a)$ for $z_0 = 0, 1a$ and $b_0 = 1a$. We also show the off-diagonal renormalization factors, which, in principle, mix with γ^0 . As expected, they are also independent of L and can be omitted in the full calculation as their contribution is negligible as compared to the diagonal contribution. Finally, we convert $B_{\Gamma}^{\text{RI-short}}$ to the $\overline{\text{MS}}$ scheme using one-loop perturbation theory,

$$B_{\Gamma}^{\overline{\text{MS}}}(z, b, \mu_0, P^z) = \sum_{\Gamma'} [Z_{\mathcal{O}}^{\overline{\text{MS}},\text{RI-short}}(z_0, b_0, \mu_0)]_{\Gamma\Gamma'} B_{\Gamma'}^{\text{RI-short}}(z, z_0, b, b_0, \mu_0, P^z). \quad (25)$$

The conversion matrix $Z_{\mathcal{O}}^{\overline{\text{MS}},\text{RI-short}}$ is calculated in dimensional regularization for arbitrary values of the momentum scale μ_0 . Explicit expressions for all Γ, Γ' are given in Ref. [51]. Similar perturbative studies can be found in Refs. [26, 33]. A comparison between the conversion factor in RI-short and the SDR scheme is shown in Fig. 11 for the case $\Gamma = \Gamma' = \gamma_0$. We observe that the real parts are compatible between the two schemes, while the RI-short scheme shows a non-zero imaginary part, in contrast to the ratio scheme. This is a consequence of using a non-zero momentum scale.

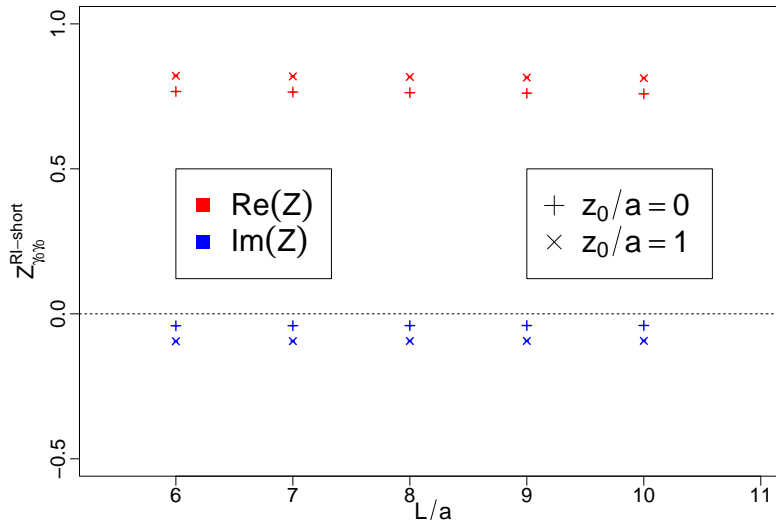


FIG. 10: The $Z_{\gamma_0}^{\text{RI-short}}$ renormalization factor within the perturbative range $b_0/a = 1$ as a function of the length L of the staple.

VI. RESULTS

In this Section, we present the renormalized beam functions in the 3 renormalization schemes discussed in Section V, as well as the corresponding results in the $\overline{\text{MS}}$ scheme.

In Fig. 12, we show the real and imaginary parts of $B_{\gamma_0}(z, b, \mu_0, P^z)$ as a function of z for two values of the transverse separation, $b/a = 1, 2$. For the real parts, the schemes agree within errors for $|z/a| \lesssim 6$. For $|z/a| \gtrsim 6$, $B_{\gamma_0}^{\text{SDR}}$ and $B_{\gamma_0}^{\text{RI-short}}$ are consistent, while $B_{\gamma_0}^{\text{RI}}$ becomes increasingly more negative with increasingly larger errors which may indicate the presence of a residual divergence in the standard RI/MOM. For the imaginary parts, we observe a similar behavior. Namely, the SDR and the RI-short schemes are almost identical for any $|z/a|$ for the two values of b/a considered. For the usual RI/MOM, we observe deviations not only for $|z/a| \gtrsim 6$ but also for most of the $|z/a|$ region with an increase in errors with increasing $|z/a|$.

The conversion to the $\overline{\text{MS}}$ scheme is done using one-loop perturbation theory for all three schemes considered. For the two cases where the renormalization factors are fixed at a short perturbative scale, we use $z_0/a = b_0/a = 1$ when computing $B_{\Gamma'}^{\text{RI-short}}(z, z_0, b, b_0, \mu_0, P^z)$ and $B_{\Gamma}^{\text{SDR}}(z, z_0, b, b_0, P^z)$. Since the final results in the $\overline{\text{MS}}$ scheme should be independent of the values we choose for the z_0, b_0 pair, we examine the stability of our results on the choice of the values for this pair. To this end, we show in Fig. 13 the product of the renormalization factors for each scheme with the corresponding conversion factors to the $\overline{\text{MS}}$ scheme, $Z_{\gamma_0}^{\overline{\text{MS}}, \text{SDR}} Z_{\gamma_0}^{\text{SDR}}$ and $Z_{\gamma_0}^{\overline{\text{MS}}, \text{RI}} Z_{\gamma_0}^{\text{RI-short}}$. These products should be independent on the choice of values of z_0, b_0 as long as the one-loop perturbative calculation is a reliable approximation. We notice that these products are equal to the renormalization factors in the $\overline{\text{MS}}$ scheme in the absence of mixing. For the ratio scheme, there is a 10% – 20% correction when going from $b_0/a = 1$ to $b_0/a = 2$ for the three values of z_0 considered here, with the correction increasing for larger values of z_0 . This indicates a limitation on the use of one-loop perturbation theory to perform the conversion to the $\overline{\text{MS}}$ scheme already at a transverse separation as low as $b/a = 2$. As a consequence, $\mathcal{O}(\alpha_s^2)$ corrections cannot be disregarded. For the z_0 dependence, the choice of $z_0/a = 0$ and $z_0/a = 1$ is nearly equivalent within one sigma error. For $z/a = 2$, the discrepancy grows, especially for $b/a = 2$. For the RI-short scheme, the situation is not significantly changed. From this discussion, we conclude that our choice for the pair z_0, b_0 is a likely safe region to fix the short perturbative scale. We show in Fig. 14 the renormalized $\overline{\text{MS}}$ matrix elements computed in the ratio and the RI-short schemes at $P^z \simeq 1.7$ GeV. The imaginary part of the matrix elements are in full agreement, the same happening in the the real part, for large z values. In the small z region of the real part there is a tendency to discrepancy, as already observed in the intermediate schemes shown in Fig. 12, although they agree within one sigma error.

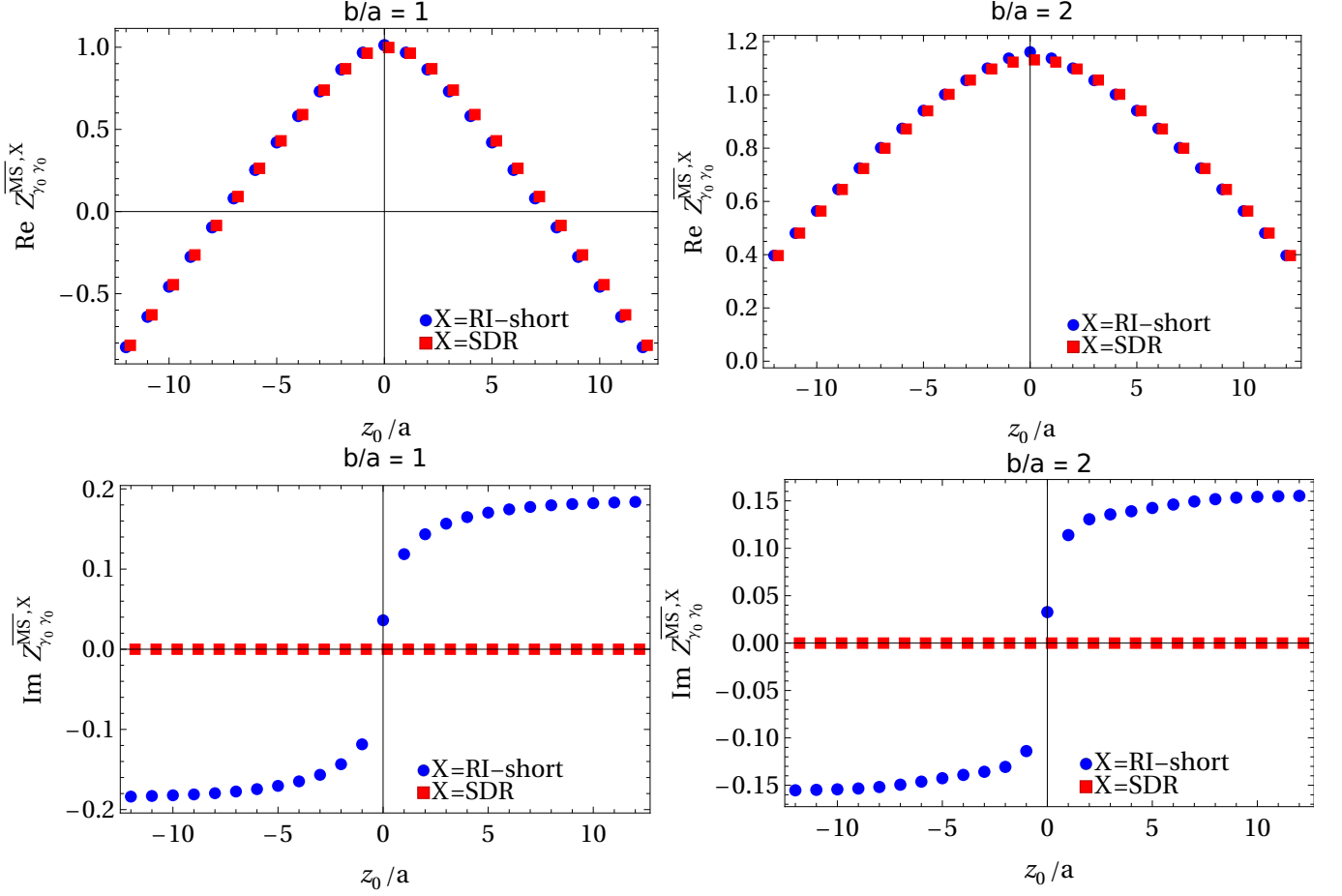


FIG. 11: Conversion factor to the $\overline{\text{MS}}$ scheme (top: real part, bottom: imaginary part) for the RI-short and SDR schemes at $b/a = 1$ (left) and $b/a = 2$ (right).

VII. CONCLUSION

In this work, we have addressed the non-perturbative renormalization of the asymmetric staple-shaped quark bilinear operators. We used symmetry arguments to restrict the possible mixing between the operators, and we found that mixing is allowed within sets of four operators. We then employed the RI/MOM scheme to estimate the importance of mixing coming from the non-diagonal terms, and we found that they can be neglected up to transverse separations of at least $6a$. This result justifies the use of multiplicative renormalization for the asymmetric staple-shaped operator. Based on this conclusion, we computed the renormalization factors in the SDR scheme, and in the RI-short scheme, where the renormalization factors are computed at short distances. We found that both schemes are nearly equivalent over all the $|z|$ region considered. Finally, we converted both schemes to the $\overline{\text{MS}}$ scheme and presented the corresponding results for the renormalized beam function. Given our previous computation of the Collins-Soper kernel and of the soft function [24], the next natural step will be to compute the TMDPDFs themselves over a wide range of b , and we plan to present results for them in the near future.

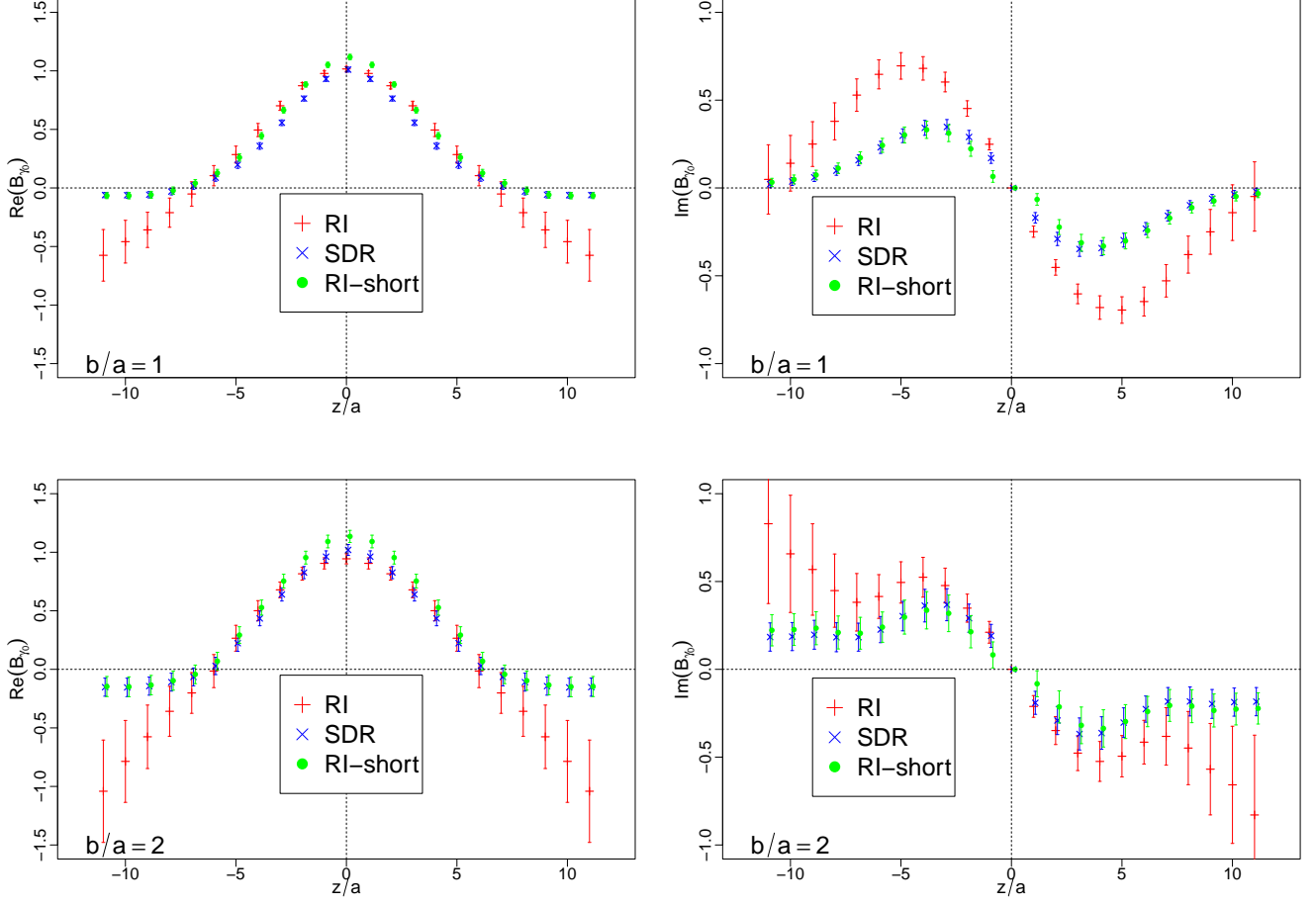


FIG. 12: Renormalized matrix elements for $z_0/a = b_0/a = 1$ for the SDR and the RI – short schemes, and $P^z \simeq 1.7$ GeV.

Acknowledgments

A.S and F.S are funded by the NSFC and the Deutsche Forschungsgemeinschaft (DFG, German Research Foundation) through the funds provided to the Sino-German Collaborative Research Center TRR110 “Symmetries and the Emergence of Structure in QCD” (NSFC Grant No. 12070131001, DFG Project-ID 196253076 - TRR 110). K.C. is supported by the National Science Centre (Poland) grant SONATA BIS No.2016/22/E/ST2/00013 and OPUS grant No. 2021/43/13/ST2/00497. M.C. acknowledges financial support by the U.S. Department of Energy, Office of Nuclear Physics, Early Career Award under Grant No. DE-SC0020405. C.A. and J.T. acknowledge partial funding from the project “Unraveling the 3D Parton structure of the nucleon with lattice QCD” (contract id EXCELLENCE/0421/0043) co-financed by the European Regional Development Fund and the Republic of Cyprus through the Research and Innovation Foundation. G.S. acknowledges funding from the European High-Performance Computing Joint Undertaking (JU) under grant agreement No. 951732 and from the European Regional Development Fund and the Republic of Cyprus through the Research and Innovation Foundation under contract No. EXCELLENCE/0421/0025. X.F. is supported in part by NSFC of China under Grant No. 11775002 and National Key Research and Development Program of China under Contracts No.2020YFA0406400. X.F and C.L. are supported in part by NSFC of China under Grant No. 12070131001. C.L. is also supported in part by NSFC of China under Grant No. 11935017, No. 12293060, No. 12293062 and No. 12293063. This work used computational resources from the John von Neumann-Institute for Computing on the Juwels booster system at the research center in Juelich, under

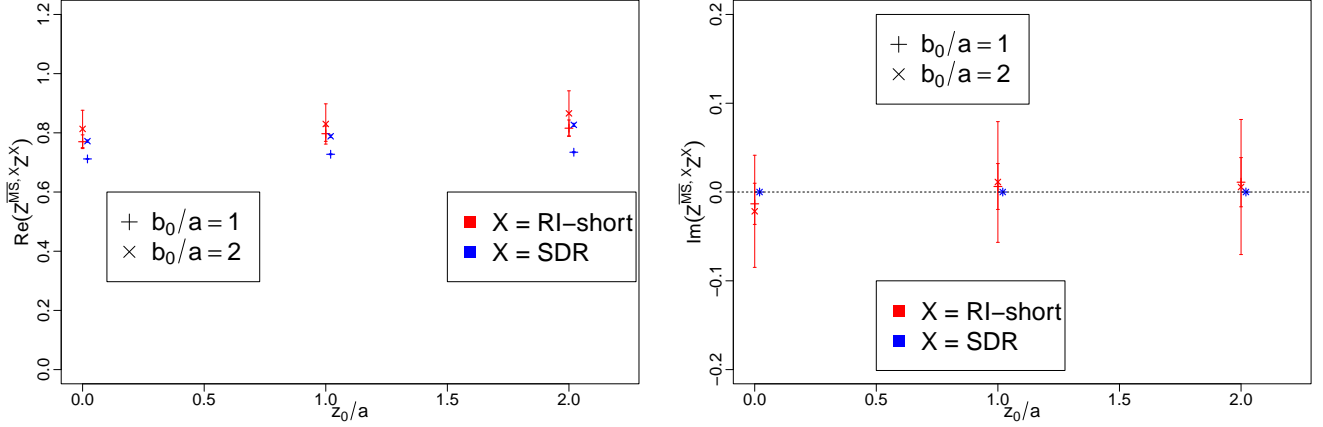


FIG. 13: Dependence of the product between the $\overline{\text{MS}}$ conversion factors and the SDR and RI – short renormalization factors on the choice of the short perturbative scale.

the project with id TMDPDF1.

-
- [1] S. Amoroso et al., *Acta Phys. Polon. B* **53**, A1 (2022), 2203.13923.
- [2] A. Bacchetta, F. Delcarro, C. Pisano, M. Radici, and A. Signori, *JHEP* **06**, 081 (2017), [Erratum: *JHEP* 06, 051 (2019)], 1703.10157.
- [3] V. Bertone, I. Scimemi, and A. Vladimirov, *JHEP* **06**, 028 (2019), 1902.08474.
- [4] I. Scimemi and A. Vladimirov, *JHEP* **06**, 137 (2020), 1912.06532.
- [5] M. Bury, F. Hautmann, S. Leal-Gomez, I. Scimemi, A. Vladimirov, and P. Zurita, *JHEP* **10**, 118 (2022), 2201.07114.
- [6] A. Bacchetta, V. Bertone, C. Bissolotti, G. Bozzi, M. Cerutti, F. Piacenza, M. Radici, and A. Signori (MAP), *JHEP* **10**, 127 (2022), 2206.07598.
- [7] P. C. Barry, L. Gamberg, W. Melnitchouk, E. Moffat, D. Pitonyak, A. Prokudin, and N. Sato (2023), 2302.01192.
- [8] J. Dudek et al., *Eur. Phys. J. A* **48**, 187 (2012), 1208.1244.
- [9] R. Abdul Khalek et al. (2021), 2103.05419.
- [10] X. Ji, *Phys. Rev. Lett.* **110**, 262002 (2013), 1305.1539.
- [11] A. V. Radyushkin, *Phys. Rev. D* **96**, 034025 (2017), 1705.01488.
- [12] K. Cichy and M. Constantinou, *Adv. High Energy Phys.* **2019**, 3036904 (2019), 1811.07248.
- [13] A. Radyushkin, *Int. J. Mod. Phys. A* **35**, 2030002 (2020), 1912.04244.
- [14] M. Constantinou, *Eur. Phys. J. A* **57**, 77 (2021), 2010.02445.
- [15] X. Ji, Y.-S. Liu, Y. Liu, J.-H. Zhang, and Y. Zhao, *Rev. Mod. Phys.* **93**, 035005 (2021), 2004.03543.
- [16] K. Cichy, *PoS LATTICE2021*, 017 (2022), 2110.07440.
- [17] K. Cichy, *EPJ Web Conf.* **258**, 01005 (2022), 2111.04552.
- [18] M. Constantinou et al. (2022), 2202.07193.
- [19] X. Ji, P. Sun, X. Xiong, and F. Yuan, *Phys. Rev. D* **91**, 074009 (2015), 1405.7640.
- [20] X. Ji, L.-C. Jin, F. Yuan, J.-H. Zhang, and Y. Zhao, *Phys. Rev. D* **99**, 114006 (2019), 1801.05930.
- [21] X. Ji, Y. Liu, and Y.-S. Liu, *Nucl. Phys. B* **955**, 115054 (2020), 1910.11415.
- [22] M. A. Ebert, S. T. Schindler, I. W. Stewart, and Y. Zhao, *JHEP* **04**, 178 (2022), 2201.08401.
- [23] Q.-A. Zhang et al. (Lattice Parton), *Phys. Rev. Lett.* **125**, 192001 (2020), 2005.14572.
- [24] Y. Li et al., *Phys. Rev. Lett.* **128**, 062002 (2022), 2106.13027.
- [25] M. A. Ebert, I. W. Stewart, and Y. Zhao, *Phys. Rev. D* **99**, 034505 (2019), 1811.00026.
- [26] M. A. Ebert, I. W. Stewart, and Y. Zhao, *JHEP* **03**, 099 (2020), 1910.08569.
- [27] P. Shanahan, M. L. Wagman, and Y. Zhao, *Phys. Rev. D* **101**, 074505 (2020), 1911.00800.
- [28] P. Hagler, B. U. Musch, J. W. Negele, and A. Schafer, *EPL* **88**, 61001 (2009), 0908.1283.
- [29] B. U. Musch, P. Hagler, M. Engelhardt, J. W. Negele, and A. Schafer, *Phys. Rev. D* **85**, 094510 (2012), 1111.4249.
- [30] B. Yoon, T. Bhattacharya, M. Engelhardt, J. Green, R. Gupta, P. Hägler, B. Musch, J. Negele, A. Pochinsky, and S. Syritsyn, in *33rd International Symposium on Lattice Field Theory* (SISSA, 2015), 1601.05717.
- [31] B. Yoon, M. Engelhardt, R. Gupta, T. Bhattacharya, J. R. Green, B. U. Musch, J. W. Negele, A. V. Pochinsky, A. Schäfer, and S. N. Syritsyn, *Phys. Rev. D* **96**, 094508 (2017), 1706.03406.

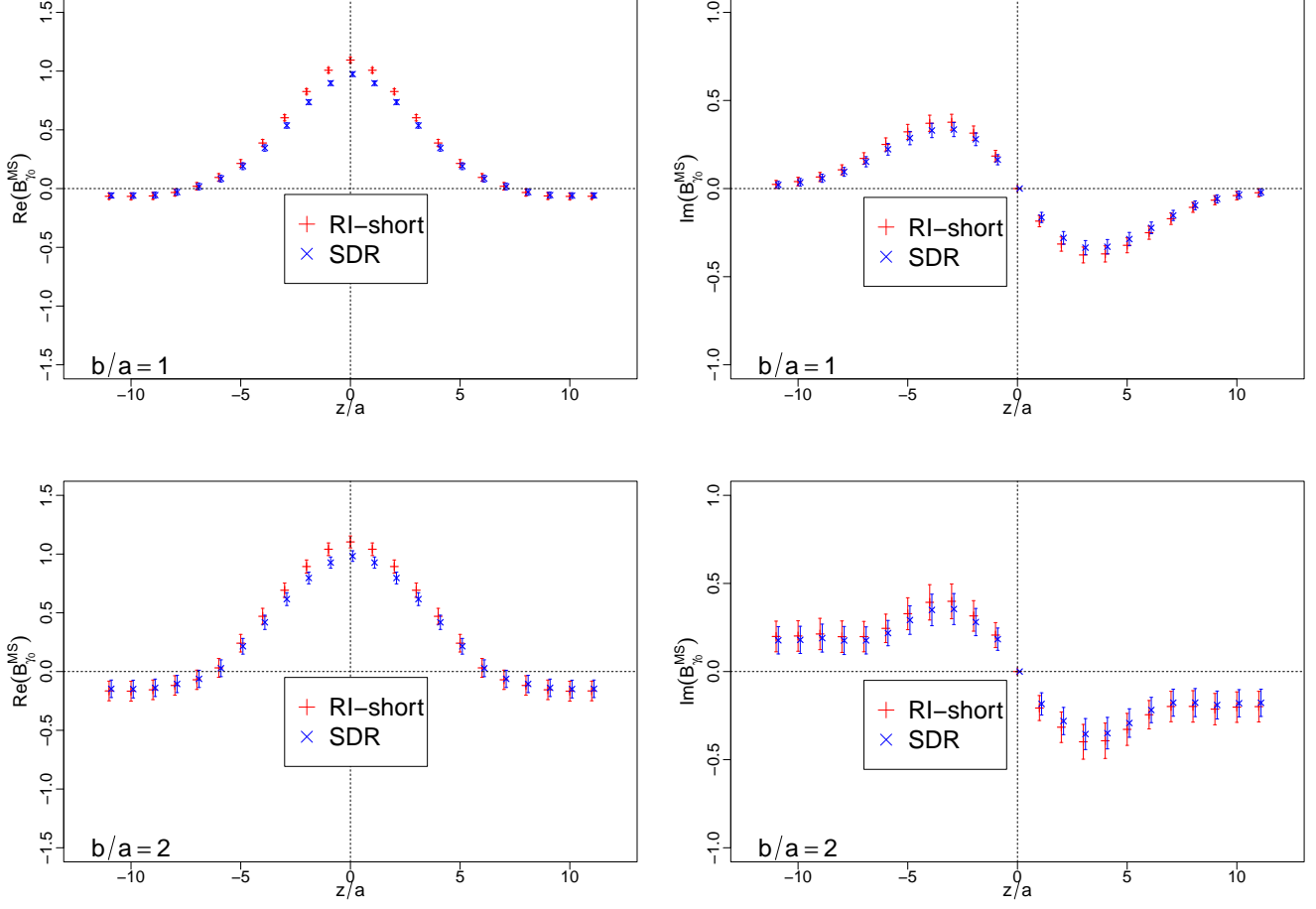


FIG. 14: $\overline{\text{MS}}$ renormalized matrix elements converted from the SDR and the RI – short schemes, using $z_0/a = b_0/a = 1$ and $P^z \simeq 1.7$ GeV

- [32] J.-C. He, M.-H. Chu, J. Hua, X. Ji, A. Schäfer, Y. Su, W. Wang, Y. Yang, J.-H. Zhang, and Q.-A. Zhang (LPC) (2022), 2211.02340.
- [33] M. Constantinou, H. Panagopoulos, and G. Spanoudes, Phys. Rev. D **99**, 074508 (2019), 1901.03862.
- [34] Y. Ji, J.-H. Zhang, S. Zhao, and R. Zhu, Phys. Rev. D **104**, 094510 (2021), 2104.13345.
- [35] M. Constantinou and H. Panagopoulos, Phys. Rev. D **96**, 054506 (2017), 1705.11193.
- [36] K. Zhang, X. Ji, Y.-B. Yang, F. Yao, and J.-H. Zhang ([Lattice Parton Collaboration (LPC)]), Phys. Rev. Lett. **129**, 082002 (2022), 2205.13402.
- [37] K. Orginos, A. Radyushkin, J. Karpie, and S. Zafeiropoulos, Phys. Rev. D **96**, 094503 (2017), 1706.05373.
- [38] V. M. Braun, A. Vladimirov, and J.-H. Zhang, Phys. Rev. D **99**, 014013 (2019), 1810.00048.
- [39] X. Ji, Y. Liu, A. Schäfer, W. Wang, Y.-B. Yang, J.-H. Zhang, and Y. Zhao, Nucl. Phys. B **964**, 115311 (2021), 2008.03886.
- [40] X. Ji, Y. Liu, and Y.-S. Liu, Phys. Lett. B **811**, 135946 (2020), 1911.03840.
- [41] J. Collins, Int. J. Mod. Phys. Conf. Ser. **4**, 85 (2011), 1107.4123.
- [42] M. G. Echevarria, I. Scimemi, and A. Vladimirov, Phys. Rev. D **93**, 054004 (2016), 1511.05590.
- [43] M. A. Ebert, I. W. Stewart, and Y. Zhao, JHEP **09**, 037 (2019), 1901.03685.
- [44] A. Shindler, Phys. Rept. **461**, 37 (2008), 0707.4093.
- [45] J.-W. Chen, T. Ishikawa, L. Jin, H.-W. Lin, J.-H. Zhang, and Y. Zhao (LP3), Chin. Phys. C **43**, 103101 (2019), 1710.01089.
- [46] C. Alexandrou et al., Phys. Rev. D **98**, 054518 (2018), 1807.00495.
- [47] G. S. Bali, B. Lang, B. U. Musch, and A. Schäfer, Phys. Rev. D **93**, 094515 (2016), 1602.05525.
- [48] G. Martinelli, C. Pittori, C. T. Sachrajda, M. Testa, and A. Vladikas, Nucl. Phys. B **445**, 81 (1995), hep-lat/9411010.
- [49] C. Alexandrou, K. Cichy, M. Constantinou, K. Hadjiyiannakou, K. Jansen, H. Panagopoulos, and F. Steffens, Nucl. Phys. B **923**, 394 (2017), 1706.00265.
- [50] J. R. Green, K. Jansen, and F. Steffens, Phys. Rev. D **101**, 074509 (2020), 2002.09408.
- [51] M. Constantinou, H. Panagopoulos, and G. Spanoudes, In preparation (2023).

[52] K. Zhang, Y.-Y. Li, Y.-K. Huo, A. Schäfer, P. Sun, and Y.-B. Yang (χ QCD), Phys. Rev. D **104**, 074501 (2021), 2012.05448.

Appendix A: Symmetry properties

As explained in Section III, we look at the mixing properties of the staple-shaped operator using symmetry arguments. We observe the transformation of the object $(ijkl)_c$, where i, j, k, l denote the signs of O^{++}, O^{--}, O^{+-} and O^{-+} respectively, and $c = \pm$ denoted the sign of the charge conjugated operators. This gives rise to 4 relevant combinations: $(++++)_c, (+-+-)_c, (++--)_c$, and $(+--+)_c$. In Table IV we summarize the symmetries of the 16 Dirac structures, where the 4 signs under any transformation denote the symmetry properties of the 4 relevant combinations, respectively.

	γ_0	γ_1	γ_2	γ_3	1	γ_5	$\gamma_5\gamma_0$	$\gamma_5\gamma_1$
$\mathcal{P}_{F_0}^{1,2}$	-+ -+	+ -+-	+ -+-	+ -+-	-+ -+	+ -+-	+ -+-	-+ -+
$\mathcal{P}_{F_1}^{1,2}$	+ -+-	-+ -+	+ -+-	+ -+-	-+ -+	+ -+-	-+ -+	+ -+-
$\mathcal{P}_{F_2}^{1,2}$	+ +--	+ +--	- -++	+ +--	- -++	+ +--	- -++	- -++
$\mathcal{P}_{F_3}^{1,2}$	+ -+-	+ -+-	+ -+-	-+ +-	-+ +-	+ -+-	-+ +-	-+ +-
$\mathcal{T}_{F_0}^{1,2}$	+ + ++	- - - -	- - - -	- - - -	- - - -	+ + ++	- - - -	+ + ++
$\mathcal{T}_{F_1}^{1,2}$	- - - -	+ + ++	- - - -	- - - -	- - - -	+ + ++	+ + ++	- - - -
$\mathcal{T}_{F_2}^{1,2}$	-+ +-	-+ +-	+ - -+	-+ +-	-+ +-	+ - -+	+ - -+	+ - -+
$\mathcal{T}_{F_3}^{1,2}$	- - ++	- - ++	- - ++	+ + --	- - ++	+ + --	+ + --	+ + --
C	c	c	c	c	$-c$	$-c$	$-c$	$-c$

	$\gamma_5\gamma_2$	$\gamma_5\gamma_3$	$\gamma_0\gamma_1$	$\gamma_0\gamma_2$	$\gamma_0\gamma_3$	$\gamma_1\gamma_2$	$\gamma_1\gamma_3$	$\gamma_2\gamma_3$
$\mathcal{P}_{F_0}^{1,2}$	-+ -+	-+ -+	+ -+-	+ -+-	+ -+-	-+ -+	-+ -+	-+ -+
$\mathcal{P}_{F_1}^{1,2}$	-+ -+	-+ -+	+ -+-	-+ -+	-+ -+	+ -+-	+ -+-	-+ -+
$\mathcal{P}_{F_2}^{1,2}$	+ +--	- -++	- -++	+ +--	- -++	+ +--	- -++	+ +--
$\mathcal{P}_{F_3}^{1,2}$	-+ +-	+ -+-	-+ +-	-+ +-	+ -+-	-+ +-	+ -+-	+ -+-
$\mathcal{T}_{F_0}^{1,2}$	+ + ++	+ + ++	+ + ++	+ + ++	+ + ++	- - - -	- - - -	- - - -
$\mathcal{T}_{F_1}^{1,2}$	+ + ++	+ + ++	+ + ++	- - - -	- - - -	+ + ++	+ + ++	- - - -
$\mathcal{T}_{F_2}^{1,2}$	-+ +-	+ - -+	-+ +-	+ - -+	-+ +-	+ - -+	-+ +-	+ - -+
$\mathcal{T}_{F_3}^{1,2}$	+ + --	- - ++	- - ++	- - ++	+ + --	- - ++	+ + --	+ + --
C	$-c$	$-c$	c	c	c	c	c	c

TABLE IV: General symmetry properties of all possible Dirac structures. The 4 signs correspond to symmetry properties of combinations $(++++)_c$ (or its equivalent $(----)_c$), $(+-+-)_c$ (or $(-+-+)_c$), $(++--)_c$ (or $(--++)_c$) and $(+--+)_c$ (or $(-+ +-)_c$). The last row indicates the symmetry properties with respect to charge conjugation (c - symmetric, $-c$ - antisymmetric).

Appendix B: Mixing sets

In this appendix we provide all the mixing sets of asymmetric staple-shaped operators with different Dirac structures, as dictated by the generalized C, P, T symmetries of Eqs. (6 – 8), in explicit form:

- $\{1, \gamma_2, \gamma_3, \gamma_2\gamma_3\}$,
- $\{\gamma_5, \gamma_5\gamma_2, \gamma_5\gamma_3, \gamma_0\gamma_1\}$,
- $\{\gamma_0, \gamma_0\gamma_2, \gamma_0\gamma_3, \gamma_5\gamma_1\}$,
- $\{\gamma_1, \gamma_1\gamma_2, \gamma_1\gamma_3, \gamma_5\gamma_0\}$.

In the case of symmetric staple-shaped operators ($z=0$), the mixing sets are reduced to:

- $\{\gamma_2, \gamma_3, \gamma_2\gamma_3\}$,
- $\{\gamma_5, \gamma_5\gamma_2, \gamma_5\gamma_3\}$,
- $\{\gamma_0, \gamma_0\gamma_2, \gamma_0\gamma_3\}$,
- $\{\gamma_1, \gamma_1\gamma_2, \gamma_1\gamma_3\}$,

while the remaining operators $1, \gamma_0\gamma_1, \gamma_5\gamma_1, \gamma_5\gamma_0$ are multiplicative renormalizable.